ELECTRICAL PROPERTIES OF RABBIT CORNEAL ENDOTHELIUM AS DETERMINED FROM IMPEDANCE MEASUREMENTS

JONG J. LIM AND JORGE FISCHBARG, *Departments of Physiology and Ophthalmology, College of Physicians and Surgeons, Columbia University, New York 10032*

ABSTRACT Alternating- and direct-current electrical characteristics of rabbit corneal endothelium were studied under varying experimental conditions. The measurements were performed by sending a 10-μA current (AC or DC) across the tissue layer. Maximal values of transendothelial potential difference and resistance were 1.3 ± 0.1 mV and 73 ± 6 $\Omega \cdot cm^2$, respectively. The short-circuit current was estimated from the potential and resistance values. Impedance loci were obtained for the frequency range 0.5–100 kHz. A capacitive reactance (C = 0.63 ± 0.02 $\mu F/cm^2$) was observed in the 100 Hz–100 kHz range. To relate the impedance data to the electrical parameters of the cell membranes, the voltage-divider ratio was determined by sending square pulses across the tissue and measuring voltage responses across the apical and basal membranes with an intracellular microelectrode. The intracellular potential difference was on the average −61 ± 1 mV, and the voltage-divider ratio was found to be between 0.33 and 4. Impedance data were fit by a computer to an equivalent circuit representing a "lumped" model, and the agreement between the model and the data was satisfactory. The results are discussed in terms of both the morphological characteristics and properties of the fluid transport mechanism across the preparation.

INTRODUCTION

This study was undertaken to gain information about the passive and active electrical properties of the corneal endothelial layer. These parameters, which were incompletely known for this tissue, are relevant to the understanding of the transport of fluid that takes place across this and other epithelia. In the present endothelial preparation, the very high ionic permeability (Maurice, 1951) and low electrical potential difference (Fischbarg, 1972, 1973; Barfort and Maurice, 1974; Hodson, 1974; Fischbarg and Lim, 1974) implied a very low electrical resistance across this preparation, and warned of possible difficulties if standard direct current analysis were used to determine electrophysiological parameters for the endothelium. The alternating-current analysis, a powerful tool originally introduced for the measurement of resistance and capacitance of cell membranes (Fricke, 1925; Cole, 1928), was therefore chosen for the purpose stated above. The technique of AC analysis has been applied to epithelia exhibiting high resistance (frog skin, Brown and Kastella, 1965; Smith, 1971; urinary bladder, Clausen et al., 1979), intermediate resistance (gastric mucosa, Dennis, 1959), and low resistance (amnion, Silver et al., 1965; corneal endothelium, Fischbarg and Lim, 1973; *Necturus* gallbladder, Schifferdecker and Frömter, 1978; Gögelein, 1980; Gögelein and van Driessche, 1981). Although the corneal endothelium belongs to the same group of leaky epithelia as the gallbladder epithelium, the magnitude of the transendothelial

resistance is lower and the preparation is more fragile than that epithelium. Hence, it was not until recently (Wiederholt and Koch, 1978; Lim and Fischbarg, 1979) that successful intracellular impalements have become possible. Thus, in this paper we report measurements of the transendothelial electrical impedance and the voltage-divider ratio as determined with intracellular microelectrodes. The results are subsequently used to put forth an electrical equivalent circuit that corresponds to a theoretical "lumped" model in terms of tissue morphology.

METHODS

Endothelial Preparation and Mounting

Corneas from female albino rabbits 3–5 kg in weight were used. The animals were killed by injecting ~5 ml of 6% Na pentobarbital through an ear vein. The method for dissection and mounting followed one previously described (Maurice, 1969; Dikstein and Maurice, 1972) with the following modifications: the ocular globes were excised, with the conjunctiva kept intact. The corneal epithelial cells were scraped off with a razor blade, and the orbital muscles and fat were dissected away. The globe, with a short conjunctival annulus attached, was then transferred to the mounting extension of one of the experimental chambers (Fig. 1), where it was held by a light vacuum. The annulus of conjunctival tissue was pulled down and tied to a groove on that extension. The globe was then cut open around the equator, the posterior half discarded, and the ciliary body, iris, and lens were pulled away. The endothelium was gently rinsed with warm (37°C) experimental solution, and the other half of the chamber was clamped in place. The inside (aqueous side) chamber was filled with solution; the pressure head imposed was ~20 cm H_2O (from aqueous to tear side). At that point, suction was discontinued and the outside chamber was in turn filled up with solution. With such a procedure, the tissue was prevented from wrinkling. The

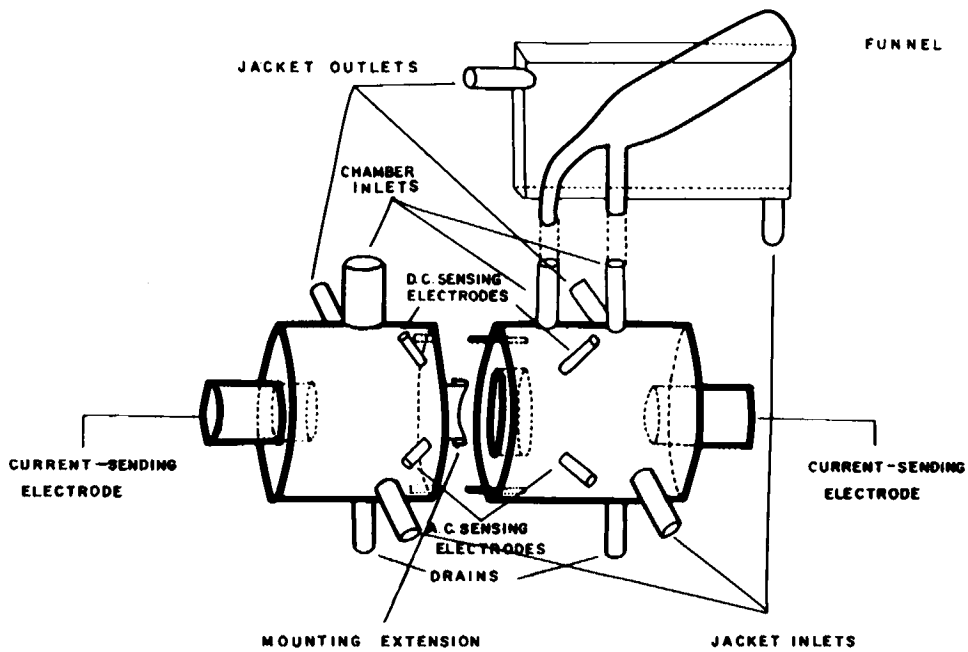

FIGURE 1 Jacketed chamber used for the potential difference, resistance, and impedance measurements. The assembly was held together by a clamp placed against the back of the current-sending electrodes.

solution in both half-chambers and funnel was kept at 37°C by circulating warm water through their jackets (Fig. 1).

Solutions

The artificial aqueous used ("regular solution," or R.S.) was similar to one developed earlier (Dikstein and Maurice, 1972), except for the inclusion of oxidized glutathione (cf. Anderson et al., 1973). It had a relatively large content of adenosine, which stimulates fluid transport across the layer (Dikstein and Maurice, 1972; Fischbarg et al., 1977). Its composition was (in mM): NaCl, 110; $KHCO_3$, 3.8; $NaHCO_3$, 39; $MgSO_4$, 0.8; KH_2PO_4, 1.0; $CaCl_2$, 1.7; glucose, 6.9; adenosine, 5.0; and oxidized gluthathione, 0.1. This regular solution was modified in some experiments by omitting some of its components; nutrients were replaced by sucrose on an osmolal basis, and HCO_3^- by Cl^-. When all three nutrients (glucose, adenosine, and oxidized glutathione [GSSG]) were absent, the solution was referred to as basal salts solution (BSS).

Measurements of Transendothelial Electrical Potential Difference

Calomel electrodes filled with 3 M KCl were connected to saline bridges filled with BSS. These bridges consisted of 3-mm o.d. glass tubes with a fritted-glass partition at the end that was immersed in the experimental chamber. Small electrical asymmetries between them were nullified with an adjustable series battery. During the experiments, when such adjustments were to be made, both electrodes were temporarily immersed in the same side of the experimental chamber. The potential difference (p.d.) was measured with an electrometer (Keithley Instruments, Inc., Cleveland, Ohio, model 610C; resolution: ± 10 μV); the electrometer output was connected to a chart recorder (Grass Polygraph, Grass Instrument Co., Quincy, Mass.). The drift of the electrode-bridge assemblies was monitored frequently during the experiments; corrections were rarely >200 μV for a typical 6-h experiment.

Transendothelial Resistance and Impedance Measurements

A four-electrode system (Fig. 2) was used for both AC and DC measurements. The electrodes with which current was passed through the preparation were made of Pb-Pb acetate to minimize polariza-

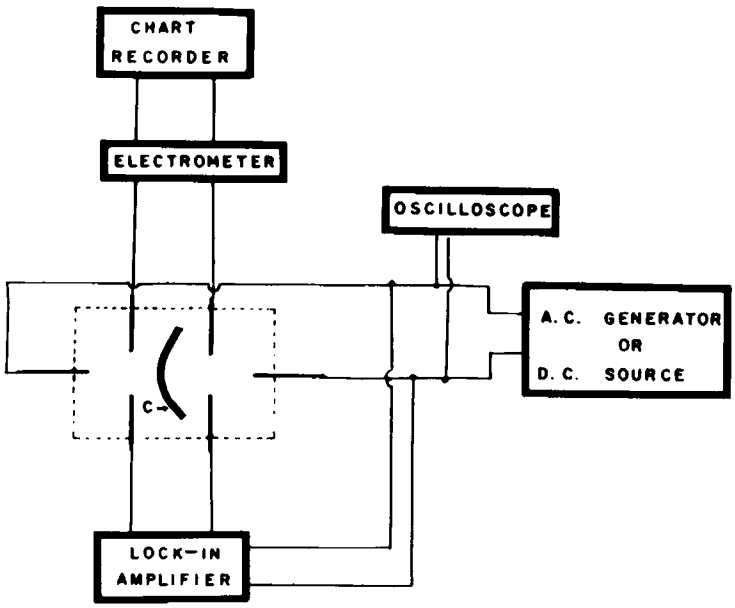

FIGURE 2 Schematic representation of the experimental setup used for the measurements of potential, resistance, and impedance. The lock-in amplifier shown was used as a vector voltmeter.

tion at low frequencies (Dennis, 1959). They consisted of layers of metallic Pb, saturated agar-Pb acetate, saturated agar-KNO_3 and saturated agar-BSS, and were placed at the far end of each chamber (Fig. 1).

The application of a direct current across the preparation induced a voltage drop, which was measured with electrodes consisting of agar-BSS filled glass capillaries. Glass tubing (rather than plastic) was used for this purpose to keep these electrodes rigidly in place. A 10-μA current was passed until a steady p.d. reading could be made with the electrometer (usually, a few seconds were required for this purpose). Typically, the shift in p.d. due to such current was ~500 μV.

For the measurements performed with AC, the electrodes that measured the voltage drop induced across the preparation had to have a relatively low resistance, since the input impedance of the preamplifier used was 1 MΩ. Chloridized Ag wires (22 gauge) placed inside capillary glass tubing (1.2 mm o.d.) were used for this purpose. The wires were glued to the glass with epoxy at the tip, with about a 1-mm length exposed. The tips of the electrodes were positioned as close as possible (~1 mm) to the preparation. A 10-μA root mean square (r.m.s.) current was again passed across the preparation, and provided adequate signal-to-noise ratio.

The 10 μA chosen for the currents was close to the expected short-circuit current for the endothelium. The currents were obtained by limiting the output of either a battery or an AC oscillator (General Radio Co., Concord, Mass., model 1310 A) with a series 100 kΩ carbon resistor. The resistance was expressed in ohms for a square centimeter of geometric area of the endothelium, which from the chamber dimensions and the corneal curvature was calculated to be 1.75 cm^2.

In early experiments, the AC voltage detected across the preparation was fed into a tuned amplifier (Princeton Applied Research Corp., Princeton, N.J., lock-in amplifier, model 8, type A preamplifier). The output of the amplifier was displayed on the *Y*-axis of an oscilloscope, while the output of the AC oscillator (reference) was displayed on the *X*-axis. Small phase differences introduced by the amplifiers were nullified before the measurements were made, and the magnitude and phase of the impedance were determined from the oscilloscope display. Later on, a more convenient and faster procedure was adopted. The signal from the experimental chamber was fed into the input of a lock-in amplifier (Princeton Applied Research Corp., model 129A), while the output from the oscillator went into the reference

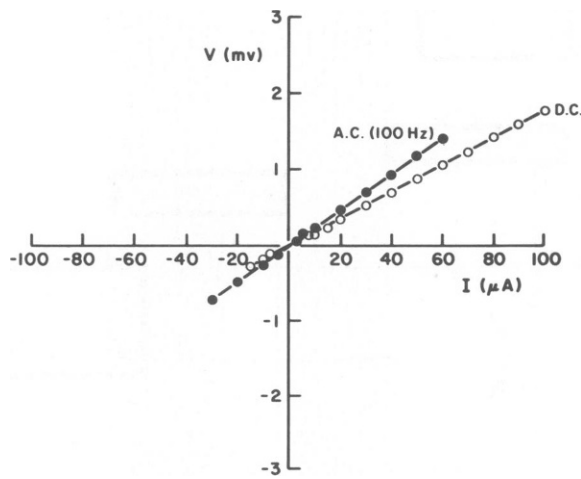

FIGURE 3 Current intensity vs. voltage plots obtained at 100 and at zero Hz (DC) in a representative experiment. In both cases, the voltage drop across the electrodes due to the solution interposed was found in the standard manner (text) and subtracted. The values shown represent current across the total 1.75-cm^2 area. The spontaneous p.d. across the endothelium was subtracted; in this experiment, it was 700 μV. The 100-Hz value was chosen because at that point the loci typically cross the real axis.

channel of that amplifier. The magnitude and phase of the impedance were read directly from the lock-in amplifier. The frequencies studied ranged between 0.5 Hz and 100 kHz.

The possible presence of artifacts that could arise from the active and passive elements used in the measuring circuit was investigated in several ways. As can be seen in Fig. 3, the behavior of the system formed by the preparation and the detection instruments was linear for both AC (100 Hz) and DC measurements for the range of current intensities employed. In another test, the behavior of the system above was investigated when passive resistive and reactive elements of suitable values were substituted for the tissue layer. When a 10-μA AC current was sent across them, the instruments yielded results that faithfully reproduced the behavior expected for those elements.

Errors coming from phase shifts that the amplifiers, electrodes, and solution could introduce were corrected as follows. Before each experiment, the chamber was filled with solution and the magnitude and phase of the impedance at all the standard frequencies employed was determined. Later on, at the end of the experiments, the chamber was open, a large hole was cut in the cornea, and the chamber was reassembled. The rigid arrangement of the electrodes prevented shifts in their position during this procedure, while the four chamber guidepins allowed us to clamp the two half-chambers (see Fig. 1) together in the same position as they had during the experiment. As a result, the values obtained before and after the experiments were quite similar. The values determined during the experiments were thus corrected by subtracting from them the corresponding values measured without the preparation in the chamber (from each impedance vector, an error vector was subtracted). Individual phase angles could be read to the nearest degree or better, and the AC voltmeter resolution was $\pm 5\ \mu$V (r.m.s.).

The transendothelial impedance characteristics were also determined by analyzing the frequency response for a pseudorandom noise current applied across the tissue. That current was obtained by converting pseudorandom noise voltage (from a Wavetek, San Diego, Calif., generator, model 132) to current with an isolation unit (W-P Instruments, New Haven, Conn., model PC1). The intensity of the current across the preparation was 60 $\mu A/cm^2$ for this case. A reference voltage was obtained across a

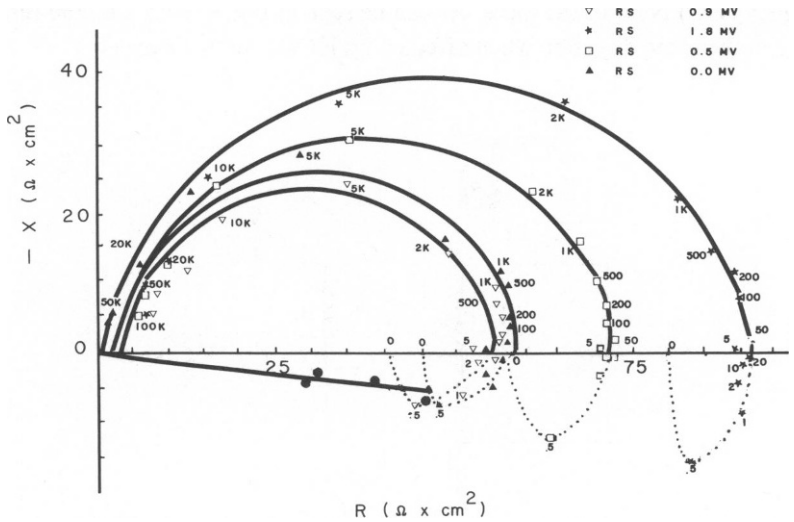

FIGURE 4 Impedance loci for the corneal endothelium supported by the stroma. Regular solution was present on both sides of the chamber. Data were taken in the sequential order (from the top downwards) shown at the upper right. Times after mounting were for the different curves: triangles, 20 min; stars, 1 h; squares, 2.5 h; and solid triangles, 5 h. The positive direction (above the real axis) represents capacitive reactance. Numbers by the experimental points denote the frequency in Hz. Curves were fitted by eye through the data. The solid circles below the real axis represent the centers of the arcs of circle that were fitted to the impedance data. These centers fall in a straight line.

10-Ω carbon resistor placed in series with the preparation. An external clock provided pulses that were used to trigger the noise generator, and to sample the voltages across the resistor and the preparation with the analog-to-digital converter of a PDP 11-34 minicomputer (Digital Equipment Corp., Maynard, Mass.). Each pseudorandom sequence lasted ~30 ms and consisted of 1,023 points. A fast Fourier transform was performed on both sets of voltage data, and the autopower spectrum of the reference voltage and the cross-power spectrum between the reference voltage and that across the preparation were obtained. Subsequently, the transfer function (impedance) was obtained by dividing the cross-power by the autopower spectrum. For these calculations, the minicomputer required ~0.5 s. To improve the signal-to-noise ratio, an average of 10 consecutive runs was taken, so that the total time for each determination was about 5 s.

RESULTS

Potential Difference, Resistance, and Impedance Locus

At the beginning of every experiment, the preparations were bathed in regular solution. Freshly mounted endothelia generated a p.d. of 1.02 ± 0.03 mV (n = 42). The initial value measured for specific resistance (called simply resistance in what follows) was 45 ± 3 Ω · cm^2 (n = 20). After the mounting, both p.d. and resistance increased, reached a maximum at 0.5–1 h afterwards, and then declined slowly during the remaining 4–5 h of useful life of the preparation. Values of maximum p.d. and resistance were, on the average, 1.30 ± 0.06 mV (n = 21; maximum value measured: 1.8 mV) and 73 ± 6 Ω · cm^2 (n = 17). A progressive decrease in resistance as a function of time can be noted also in Fig. 4. As explained in the Discussion, the total resistance across the endothelial layer (R_1, Fig. 5 *a*) can be taken to correspond to the segment on the real (R) axis between the high frequency intercept and the zero frequency (DC) point of the locus. As can be seen in Fig. 6, both p.d. and resistance also tend to vary in the same direction when affected by HCO_3^- substitutions.

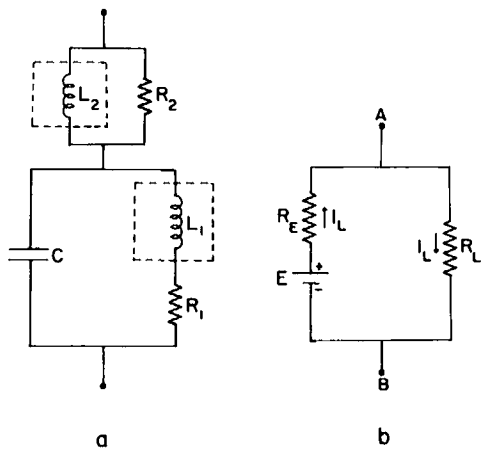

FIGURE 5 (*a*) Equivalent electrical circuit diagram, simplified to the minimum, representing the corneal endothelial preparation. The relationship proposed between the different elements and the morphology of the preparation is shown in Fig. 13. The elements shown inside the rectangular boxes (dashed) are "apparent" ones and hence are not shown in Fig. 13. (*b*) Simplified equivalent circuit representing some of the elements postulated for an active ion transport mechanism across the corneal endothelium. E, electromotive force of the pump; R_E, internal resistance of the pump and cell membranes in series; R_L, resistance of the leak pathway.

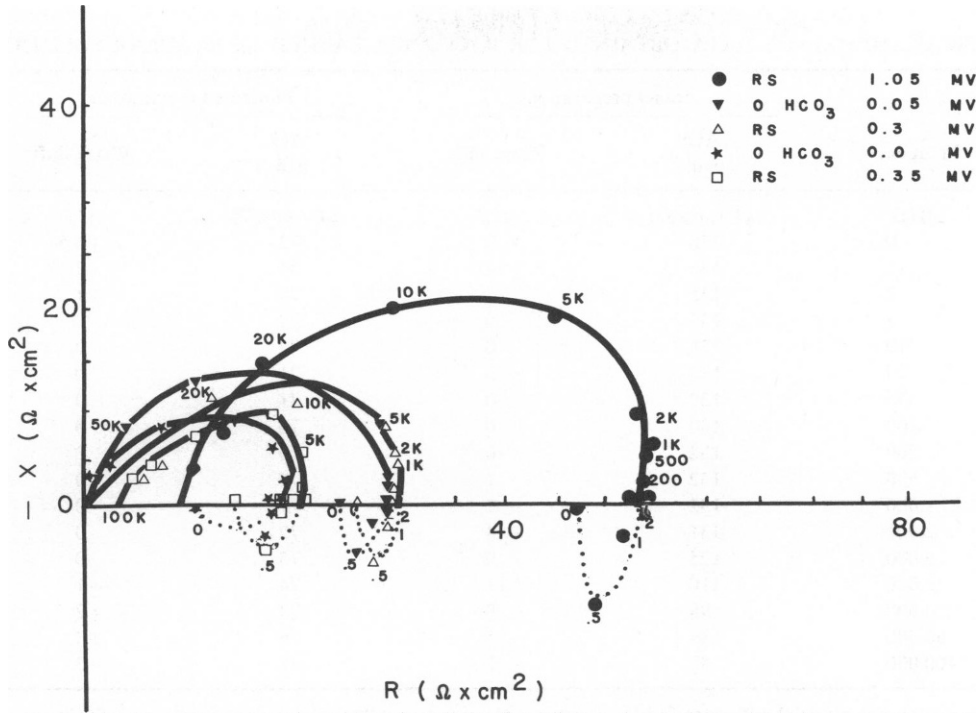

FIGURE 6 Comparison of impedance loci obtained with regular solution and with HCO_3^--free solution. Curves were determined sequentially in the same experiment, in the same order as the symbols are listed.

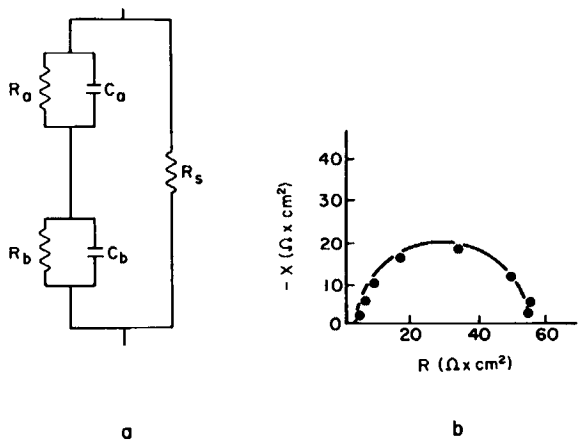

FIGURE 7 (*a*) An equivalent circuit postulated for the corneal endothelium (lumped model); *R* and *C* represent the resistance and capacitance, and the subscripts a, b, and s stand for the apical and basal cell membranes and for the shunt pathway, respectively. (*b*) Impedance locus of corneal endothelium: the dots correspond to the points determined in a representative control experiment, while the broken solid lines were obtained by fitting the same experimental points to the equivalent circuit shown in (*a*).

TABLE 1

TYPICAL IMPEDANCE DATA OBTAINED FOR A CORNEA BATHED IN REGULAR SOLUTION

Frequency	Intact preparation		Punctured preparation	
	AC p. d.	Phase shift	AC p. d.	Phase shift
(Hz)	*(μV r.m.s./2)*	*(°)*	*(μV r.m.s./2)*	*(°)*
0.5	130	+ 9	72	+6.5
1	133	+ 4	74	+3
2	135	+ 1.5	74	+1
5	135	0	73	0
10	134	0	72	0
20	133	0	71	0
50	132	0	71	0
100	132	0	70	0
200	132	0	70	0
500	132	− 1	70	0
1,000	132	− 2	71	0
2,000	131	− 4	72	0
5,000	125	− 9	73	0
10,000	110	−11	74	+1
20,000	98	− 9	74	+2
50,000	89	− 5	76	+3
100,000	87	− 2	77	+3

Transendothelial potential difference and DC resistance measured were 900 μV and 51 Ω · cm^2, respectively.

From the figures presently reported for p.d. and the total tissue resistance (R_1; cf. Fig. 5), the short-circuit current (s.c.c.) that would have existed at those times can be estimated. The value of R_1 includes in principle the shunt due to possible edge damage (Helman and Miller, 1971), but in a previous study done with this preparation (Fischbarg et al., 1977), whatever degree of edge damage there might have been was found not to result in measurable fluid leaks across the tissue. Therefore, edge damage effects were neglected in our study. In consequence, as a corollary of the model proposed in Figs. 5 and 7, the s.c.c. can be expressed

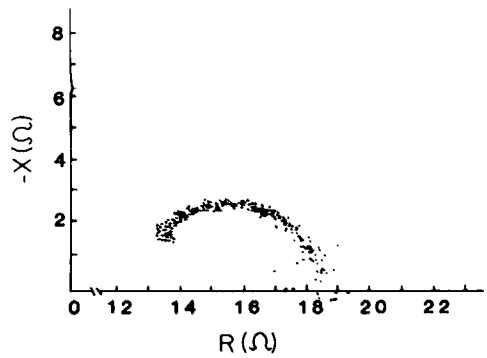

FIGURE 8 Impedance locus of the corneal endothelium. A pseudorandom noise current pulse was applied across the endothelium. The transendothelial voltage response due to such current was processed by a computer to calculate the transfer function, from which the impedance locus was finally obtained. In this case, the solution contained neither adenosine nor gluthathione.

as the ratio between p.d. and R_1. In that context, the value of R_1 experimentally measured results from the parallel combination of the shunt resistor with the cell membrane resistance (cf. Fig. 5 *b* and its legend). At open circuit, the current circulating around the loop in Fig. 5 *b* (I_L) represents the ionic flows that make up the net flow of salt across the preparation. In general, the relation between I_L and the short-circuit current I_{sc} would be given by: $I_{sc}/I_L = (R_L + R_E)/R_E$, but in the present case, since R_E is likely to be >1,000 Ω · cm^2, the use of I_{sc} as an estimate of I_L would introduce an error of ≤7%. Since this is of the order of the standard error for the resistance (R_1) data, this estimate will be used in what follows. The s.c.c. thus calculated increased after mounting, reached a maximum ~1 h afterwards, remained relatively stable for another hour, and then decreased slowly. As a quantitative example, the values for the four successive determinations in 5 h for the experiment shown in Fig. 4 were: p.d., 0.9, 1.8, 0.5, and 0 mV; R, 38, 78, 55, and 42 Ω · cm^2; and s.c.c., 23, 23, 9, and 0 μA/cm^2, respectively. On the average, the values calculated in this fashion for the s.c.c. come out to be 23 ± 2 μA/cm^2 initially and 18 ± 2 μA/cm^2 at maximal p.d.

The characteristics of the endothelial impedance were explored in some 16 experiments. Table I shows a set of data from a representative experiment. In addition, Figs. 4, 6, 8, and 9 show other examples for which Nyquist plots were chosen for the impedance data so as to display their locus. As expected, the loci are close in shape to arcs of circle, although, as discussed below, some deviation is apparent. In addition, in some of the figures (cf. Fig. 4), the high-frequency intercept of the real axis does not coincide with the origin. This suggests that, even after subtracting for the resistance of the solution interposed between the electrodes, another resistance in series with the preparation remains, which probably arises in the stroma.

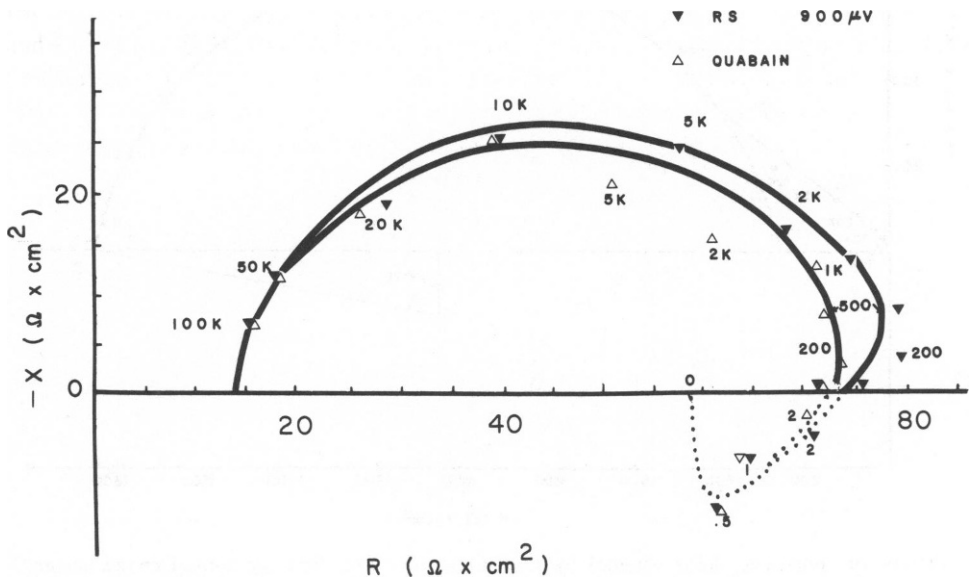

FIGURE 9 Impedance loci obtained with regular solution (solid triangles) and after the addition of 10^{-5} M ouabain (open triangles). Two examples are presented. The values of the potential difference before ouabain was added are shown at the upper right.

Fig. 8 shows an example of the data obtained by passing a pseudorandom noise current across the preparation. The data are in close agreement with those obtained with the lock-in amplifier at comparatively low and medium frequencies. High-frequency data could not be properly collected, owing to the bandwidth limitation of the particular amplifier used, which had been designated for work in *Necturus* gallbladder epithelium (Suzuki et al., 1978; Lim et al., 1980); that tissue has higher total resistance than the present preparation.

For the purpose of comparison, the impedance locus for the corneal epithelium was also determined. Since the epithelium has several layers of cells and is a tight tissue known to possess a resistance of the order of kilohms for a square centimeter, one might expect its impedance locus to be different from that of the endothelium. This expectation was confirmed, as shown in Fig. 10. In addition, by extrapolating a circular arc at the higher frequency values up to the real axis (dotted line in the figure), the transepithelial resistance can be estimated. The value thus obtained is ~1.6 kΩ · cm^2, which is the lower limit of the values found for that tissue, viz., 1.6–3.9 kΩ · cm^2 (Klyce, 1972); 9.1 ± 0.5 kΩ · cm^2 (Klyce and Wong, 1977).

Experiments Involving Replacement of Ambient Solutions

The usual protocol consisted of measuring p.d., resistance, and impedance during an initial 1–1.5-h period, and then replacing the regular solution by the one being tested. Suction applied to the outer side of the cornea prevented it from wrinkling while the solution on the inside was being exchanged.

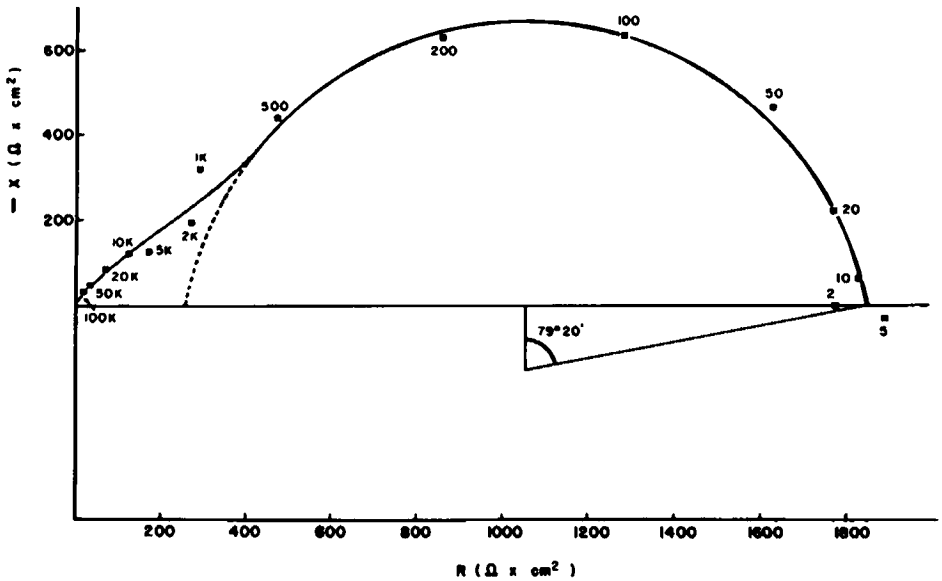

FIGURE 10 Impedance locus obtained by sending current across both the corneal epithelium and endothelium in series. The frequency of maximum capacitive reactance is lower than that in the case of the endothelium alone, owing to the higher resistance of the epithelial layer. The deviation from the circular arc at the high frequency end (>500 Hz) can be attributed to the presence of the endothelium.

Effects of Bicarbonate-free Solutions

The p.d. was monitored at regular intervals after mounting. After 0.5–1 h, the p.d. usually reached its near-maximal value for a given experiment. At this point, impedance data were recorded. Subsequently, the bathing solution on both sides of the preparation was replaced by a bicarbonate-free solution. The p.d. was monitored for a short period (~5 min) and impedance data were again recorded. After these measurements, the bicarbonate-free solution was replaced by regular solution, and data were recorded once more. The sequence of measurements above could be repeated three or four times during the useful life of a preparation. Fig. 6 shows one such experiment. Note that the resistance fell noticeably after regular solution replaced the bicarbonate-free solution. Upon returning to regular solution, both p.d. and resistance recovered partially. Average values for the estimated short-circuit current (see below) are shown in Fig. 11 together with those for p.d. and resistance (R_t) at each point. The s.c.c. is clearly seen to fall after bicarbonate-free substitution, but to recover towards values near those of the initial period when the test solution was replaced by regular solution.

Effects of Ouabain

As above, the test solution was used after a period of equilibration. Ouabain was added to the inside chamber up to a final concentration of 10^{-5} M; p.d. was measured and impedance data were recorded. The p.d. was immediately abolished, as shown earlier (Fischbarg, 1972, 1973), but the resistance either showed no change (Fischbarg and Lim, 1973) or decreased slightly. In addition, ouabain treatment mitigated whatever eccentricity had been previously present. Fig. 9 shows an experiment representative of the nine performed.

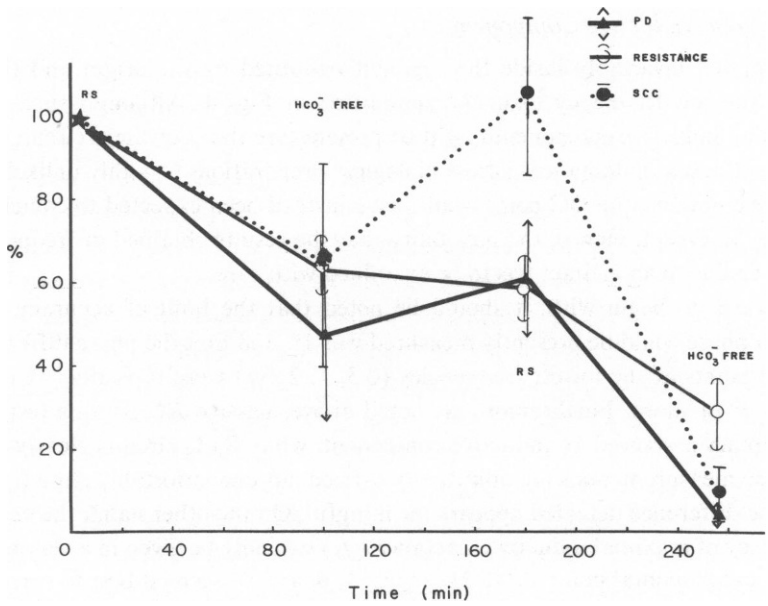

FIGURE 11 Plot of p.d., resistance, and s.c.c., as a function of time. Average values and their SEM are expressed as percentages of each initial value for a given experiment.

Capacitance

A capacitive reactance was observed in every case in which the endothelial cell layer exhibited normal p.d., and was eliminated by scraping off the cells. This reactance appeared in the locus as an arc of circle, except for the slight eccentric deviations noted elsewhere in the text. Arcs fitted graphically to the experimental points were generally centered below the real axis (cf. Fig. 4), as has been seen in many other previous instances (Cole, 1968). Although the origin of such depression is not completely known, the polarization angle was operationally defined, as customary (Brown and Kastella, 1965), as $\sin \theta = d/r$, d being the distance from the real axis to the center of the circle and r being the radius of the circle. In the present results, this angle was 8.7° ± 1.4 (n = 30; range 2–25°). Its value remained constant throughout each given experiment, in spite of changes in the ambient solutions.

The frequency of maximal capacitive reactance (characteristic frequency f_C) was read by eye from each graph. By relating the characteristic frequency to the equivalent time constant ($\tau = RC$), a value for the effective capacitance C was obtained. Fig. 4 shows that the value of f_C increased as R_1 decreased. In the equivalent circuit discussed below (cf. Fig. 5 *a*), this would be expected if the value of the parallel capacitance (C) across the endothelium would remain constant, since $f_C = 1/2\pi (R_1 C)$ in terms of that model. This expectation was confirmed by the results; the calculated value for C changed little or not at all for a given preparation, regardless of which experimental manipulation was performed. For example, in the experiment shown in Fig. 4, the values for C were 0.55, 0.66, 0.58, and 0.58 $\mu F/cm^2$ for the four successive series of measurements. The average of C for all the measurements done was 0.63 ± 0.02 $\mu F/cm^2$ (n = 107). One should note that this simple and useful estimate is possible from a Nyquist plot, but not directly from a Bode plot.

Apparent Inductive Component

The DC point fell invariably inside the segment delimited by the origin and the real axis intercept at the low-frequency end, as exemplified in Fig. 4. Although such a deviation suggests that an inductive component might be present (see the equivalent circuit in Fig. 5 *a*), the existence of actual inductances across biological preparations is highly unlikely. Based on simple intuitive notions, the DC point would have instead been expected to coincide with the low-frequency intercept. Hence, the possibility that the results obtained at frequencies below 10 Hz could be due to an artifact has to be examined with care.

In this regard, to begin with, it should be noted that the limit of accuracy with which differences in phase could be presently measured was 1°, and that the phase differences of the experimental points at the lowest frequencies (0.5, 1, 2 Hz) were typically +1 or +2°, and sometimes +3° or more. Furthermore, as noted above, passive RC circuits tested with the present set-up never showed an inductive component, while RLC circuits clearly did. Hence, although these measurements were admittedly carried out uncomfortably close to the limit of resolution, the difference detected appears meaningful. On the other hand, the determination of the frequency of maximal inductive reactance (f_L) can only be given in a very approximate fashion. The experimental point at 0.5 Hz (Figs. 4, 6, and 9) seemed best to correspond with f_L, but this happened to be the lowest frequency to which the lock-in amplifier would respond. In balance, the effect appears real in the present data, although some uncertainty is bound to

remain until an alternative, more sensitive technical procedure can be developed for this purpose.

Eccentricity

In about half of the experiments, the impedance loci deviated from the shape of an arc of circle and were instead eccentric at relatively low frequencies (20 Hz $< f <$ 2 kHz). This eccentricity is apparent in the experiments shown in Figs. 6 and 9. In addition, in several of the experiments in which substitution with HCO_3^--free solution was performed, the eccentricity decreased after the substitution, only to become noticeable again upon returning to regular solution. An example is shown in Fig. 6, and possible explanations for these observations are discussed below.

Voltage Divider Ratio

Using conventional microelectrodes, we performed 23 cellular impalements in three endothelial preparations. The intracellular potential was -61 ± 1 mV (range: 45–88 mV; $n = 16$). In eight of these impalements, the voltage divider ratios ($\Delta V_{apical}/\Delta V_{basal}$) were determined by sending square pulses (58 $\mu A/cm^2$ current, 10 s duration) across the endothelium with two external electrodes, while the microelectrode recorded the voltage drop induced by the current pulses. In the typical example shown in Fig. 12, the microelectrode is at first on the aqueous side; subsequently, it is advanced into the cell, and, finally, it exits the cell at the stromal side.

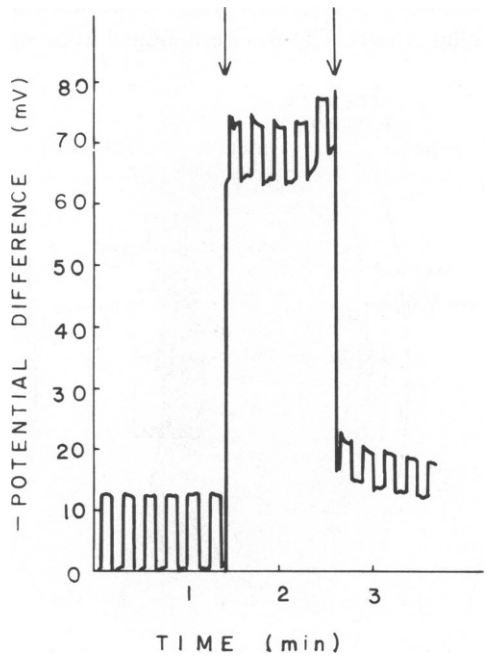

FIGURE 12 The voltage divider ratio. A microelectrode was advanced from the aqueous side at first into the cell (arrow at left) and subsequently into the stroma (arrow at right). The voltage responses shown are due to a current pulse applied across the tissue.

The voltage drop induced by the current pulse was measured at each position of the microelectrode. The value at the last position represented the drop across the stroma, and was used to correct the other values. In that fashion, $\Delta V_{\text{transendothelial}}$, ΔV_{basal}, and hence the voltage divider ratio could then be obtained. The average value thus found for that ratio was 1.0 ± 0.3 (n = 8, range: 0.33–4).

Curve-fitting

Results from some of the experiments in which the preparation had been bathed with regular solution were selected for curve-fitting. An equivalent circuit (Fig. 7 *a*) was drawn by analogy with tissue morphology (cf. Fig. 13). The equation describing the behavior of that circuit is given in the Appendix. Since such model predicted loci of circular shape, experiments were chosen for which the results did not exhibit eccentric deviation. To test the agreement between the data and the model, a curve satisfying such equation (cf. Appendix) was fit to the experimental data by least squares using a finite difference Levenberg-Marquardt algorithm incorporated into a Fortran program. Subroutines used for this purpose were the VA05A from the Harwell Subroutine Library (Atomic Energy Research Establishment, Harwell, Oxfordshire, England) and the ZXSSQ from the International Mathematical and Statistical Libraries, Inc., Houston, Tex. Both yielded similar results. For the particular experiment shown in Fig. 7 *b*, the best fit was obtained with the following set of parameter values: R_a = 1.58 kΩ · cm^2; R_b = 1.53 kΩ · cm^2; R_s = 67 Ω · cm^2; C_a = 1.03 μF/cm^2; C_b = 1.03 μF/cm^2. The subscripts a, b, and s stand for the apical and basolateral cell membranes, and for the paracellular shunt, respectively. This curve-fitting procedure was done for four other experiments, with very similar results. The fits were judged to be satisfactory on the basis of

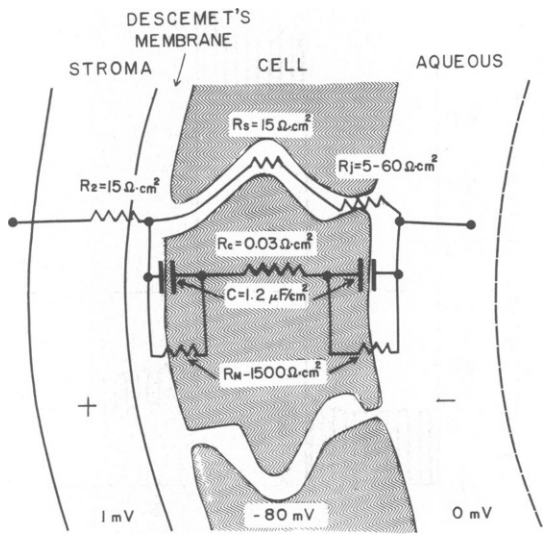

FIGURE 13 Schematic morphological representation of the corneal endothelium with the corresponding equivalent electrical parameters at the locations postulated. R_M, cellular membrane resistance; R_S, resistance of the intercellular space; R_J, resistance of the intercellular junctions; R_2, resistance of the stroma; C, capacitance of the cell membrane; R_C, resistance due to the cytoplasm. The figures shown are based on values either experimentally measured or estimated.

visual inspection alone. This procedure was further validated by the fact that the differences between the experimental and theoretical values of the real (R) and imaginary (X) components were very small upon convergence. For the experiment given in Fig. 7 *b*, the average deviation, $\Sigma[(\Delta R/R) + (\Delta X/X)]/2n$, was <1%.

A comparison can be made between the results of the curve-fitting procedure and the estimates of the same parameters obtained from the present experimental results. As can be seen from the data given elsewhere in the paper (Fig. 12), the average voltage-divider ratio was ~1, and the effective capacitance across the tissue calculated from the time constants was 0.63 $\mu F/cm^2$. Both of these values agree reasonably well with the values derived from the fit to the equivalent circuit above.

DISCUSSION

P.D., Resistance, S.C.C., and Water Flow

In previous publications, the value reported for the transendothelial potential difference has ranged from 0.5 to 1.3 mV (Fischbarg, 1972, 1973; Barfort and Maurice, 1974; Hodson, 1974; Fischbarg and Lim, 1974). In the present experiments, adenosine was included in the ambient solutions, which could account for the value of 1.02 mV reported here. Such value agrees quite well with the value that Barfort and Maurice (1974) found under similar conditions. In our own previous papers, the values we have reported in the presence of adenosine were somewhat lower than the present ones. This might be due to the fact that the 37°C temperature control in the present chamber is much improved. On the other hand, when only glucose (and no adenosine) is present as a nutrient, p.d. values have been reported to be lower (540 ± 20 μV, Hodson, 1974; 590 ± 35 μV, Fischbarg, 1979). For the sake of completeness, it will be also mentioned that the fall in p.d. with bicarbonate-free solutions has been reported before (Fischbarg, 1972, 1973; Fischbarg and Lim, 1974; Hodson, 1974).

Values of electrical resistance have not been apparently determined in the presence of adenosine so far, except in our own previous work (Fischbarg and Lim, 1973), and are presently reported to range between 45 and 60 $\Omega \cdot cm^2$. Note, however, that when the only nutrient present is glucose (with no adenosine), the total tissue resistance is lower (20 $\Omega \cdot cm^2$, Hodson and Miller, 1976; Fischbarg, 1979). It is also worth noting that, as reported here, the resistance falls in the presence of bicarbonate-free solutions.

The model in Fig. 13 details the morphological basis for the equivalent circuit elements postulated. The values for those elements have been either experimentally determined or estimated (Fischbarg and Lim, 1973). As proposed elsewhere (Fischbarg, 1973), a solution-filled hexagonal maze composed of the intercellular spaces and the apical junctions in series would have an electrical resistance of ~22 $\Omega \cdot cm^2$. As mentioned above, such values are found in the presence of glucose or in bicarbonate-free solutions, whereas in the presence of adenosine the resistance is larger. The results are therefore consistent with the possibility that an increased rate of pumping would result in a relative decrease in the width of the intercellular spaces. Since the endothelium is a secretory or "backwards" epithelium (Diamond and Bossert, 1968), the implication is that water would be taken up by the cells from a hypotonic intercellular space, which would tend to cause the decrease in width postulated.

The values of 23 and 18 $\mu A/cm^2$ calculated here for the initial and steady-state s.c.c. could be equivalent to the net transendothelial ionic flows of 0.86 and 0.67 $\mu eq/h \cdot cm^2$, respectively. It is not clear, however, whether the estimated s.c.c. agrees with the net ionic fluxes, since recent measurements of net ionic fluxes across the endothelium using radioisotopes have yielded somewhat conflicting results. Thus, the net HCO_3^- flux has been reported to be ~0.7 $\mu eq/h \cdot cm^2$ under short-circuit (Hodson and Miller, 1976), and 2.51 ± 0.21 $\mu eq/cm^2$ (Hull et al., 1977) at open circuit. As for Na^+, a net flux of 2.3 $\mu eq/h \cdot cm^2$ at open circuit has been recently reported (Lim, 1981*a*, *b*). Since the rate of fluid transport experimentally determined is on the order of 4.0–6.0 $\mu l/h \cdot cm^2$ (Maurice, 1972; Fischbarg et al., 1977), net ionic fluxes of $> \sim 1.0$ $\mu eq/h \cdot cm^2$ imply that the fluid transported is hypertonic. Clearly, more work is needed to resolve this issue.

Reactive Elements

Capacitance values similar to the one reported here have been found in other studies of epithelia (Teorell, 1949; Dennis, 1959; Silver et al., 1965). Other characteristics seen here, such as the displacement of the center of the loci below the real axis and the constancy of this polarization angle, have been described at length before (Cole, 1965; Schwan, 1957) and have been attributed to dielectric polarization (Brown and Kastella, 1965). Since the (monocellular) endothelial layer has a simple geometry, it seems reasonable to asume that the effective capacitance of 0.63 $\mu F/cm^2$ across such layer is due to the capacitance of two similar cell membranes in series (Fig. 7). Since the basolateral membrane area is ~2.4 times that of the apical one, the capacitance for each cell membrane should be 0.89 $\mu F/cm^2$ of membrane area. This figure is close to the ~1 $\mu F/cm^2$ value ubiquitously found for cell membranes ever since it was first determined (Fricke, 1925; Cole, 1928). Note that the corneal endothelial apical cell membrane has a rather flat surface in comparison with the microvillae and foldings found in, for instance, gallbladder (Schifferdecker and Frömter, 1978) and urinary bladder cells (Clausen et al., 1979). Hence, the 0.89-$\mu F/cm^2$ value reported here is consistent with the present geometry, whereas the values of 7–20 $\mu F/cm^2$ that the above authors reported corresponds to the larger cell membrane area derived from folding in their cases. While on this subject, we should note that the validity of the lumped model shown in Fig. 7 *a* may be questioned, because Clausen et al. (1979) have shown that a distributed model fitted their experimental data better than a lumped one (the term "distributed" as applied to an epithelial model was first used by Frömter [1972]). There are, however, morphological differences between the urinary bladder or gallbladder and the corneal endothelium, since the lateral foldings in the endothelium appear to be less extensive (Kaye and Pappas, 1962; Hirsch et al., 1976). Hence, the lumped model provides an approximation of sufficient accuracy for the purposes of the present analysis, as can be gathered from the close agreement between the present data and the models in Figs. 5, 7, and 13.

Eccentricity

Another interesting aspect of many curves was the eccentric deviation from their circular shape described above (Figs. 6 and 9). Even if the deviations were sometimes subtle, in experiments such as those shown in Figs. 6 and 9 they were seen to decrease or disappear when the transport mechanism was impaired (even twice during an experiment; cf. Fig. 6). Several

explanations for the meaning of these deviations may be offered. First, if the time constants for the apical and basal membranes were different, their impedance loci would appear as separate arcs. As the time constants would become closer, "fusion" would develop between the arcs, so that the experimental curve might actually be composite, and hence eccentric. In addition, the paracellular pathway would act as a shunt for the apical and basal membranes and would be expected to modify the impedance of the system. In this connection, an interesting theoretical prediction has been made by Schifferdecker and Frömter (1978) for a case in which the shunt resistance would be relatively high owing to collapse of the intercellular spaces. As can be seen in their Fig. 11 ($r = 0.1$ and $r = 0.05$), the eccentric behavior becomes less pronounced as the shunt resistance decreases. As detailed above, however, the time constants found for the present case, which would correspond to the apical and basolateral membranes, are similar in value, so that a complete explanation in the terms above appears doubtful. Another explanation would be that an anomalous reactance (or apparent inductance) would be present across the endothelium, anomalous in the sense that no passive physical properties of the endothelium would otherwise explain it. Its possible theoretical location would be in series with the paracellular shunt resistor, as shown in Fig. 5 in dashed lines (L_1; value: 10^{-4}–10^{-3} H · cm^2). As for its possible origin, it may be speculated that an ionic gradient along the paracellular pathway could account for it. In this framework, by using the above range for L_1 as an estimate and calculating the parameters for an ionic redistribution process (Cole, 1965), the characteristic length along which an ionic gradient would result in this behavior is 7–8 μm, which is of the order of the cell thickness (5 μm) or the length of the intercellular spaces (12 μm). On balance, however, it appears that this issue will have to be reexamined with faster and more accurate methods before a more definitive assessment of its meaning can be offered.

As for the reactive component seen below the real axis, it was found usually between 10 and 0.5 Hz (shown in the dotted lines in Figs. 6, 7, and 8). Since this last value represents the very limit of resolution of the lock-in amplifier used, further investigation in the low frequency domain with alternative methods appears desirable. Still, the technical reservations that can be made about the present results are tempered by two facts: (*a*) a similar behavior was seen by simply calculating the impedance from Lissajous patterns on an oscilloscope (Fischbarg and Lim, 1973); and (*b*) in the present results the DC point fell always closer to the origin than the low-frequency crossing of the real axis (the typical low frequency at that intersection was 100 Hz, for which the amplifier response was quite adequate). If the reasoning above is repeated and ionic gradients are again invoked as an explanation for this anomalous reactance, the characteristic length that can be calculated for such an effect here would be of ~80 μm. This order of magnitude seems to point to either the stroma (600 μm thick when swollen) or the unstirred layers in contact with the tissue as possible sites for them. Anomalous reactances have been experimentally observed (Cole and Baker, 1941; Cole, 1949; Teorell, 1949) and theoretically analyzed (Cole, 1965, 1968). In particular, for the case in which a bi-ionic gradient exists across a membrane, there are both a theoretical prediction (Sandblom, 1972) and an experimental confirmation (Gögelein, 1980; Gögelein and van Driessche, 1981) of the existence of an anomalous (inductive) reactance. Sandblom solved the time-dependent Nernst-Planck equation and Poisson's equation. From the solutions obtained, he predicted that both an inductive and a capacitive reactance could appear across a membrane, depending

on the magnitude and orientation of the external ionic gradient. In turn, Gögelein and van Driessche (1981) observed an inductive behavior when their gallbladder preparation was bathed with KCl-Ringer's solution on the serosal side and with NaCl-Ringer's solution on the mucosal side. The conditions under which such effects could appear in the present preparation will need further exploration.

APPENDIX

The equation for the impedance of the circuit shown in Fig. 7 *a* is

$$Z = \frac{R_a(1 + \omega^2\tau_b^2) + R_b(1 + \omega^2\tau_a^2) - j\omega[R_a\tau_a(1 + \omega^2\tau_b^2) + R_b\tau_b(1 + \omega^2\tau_a^2)]}{(1 + \omega^2\tau_a^2)(1 + \omega^2\tau_b^2)},$$

where $\tau_a = R_aC_a$, $\tau_b = R_bC_b$. R_a, R_b, C_a, and C_b are defined in the legend of Fig. 7 *a*. The data experimentally obtained were fitted to the equation above.

Dr. Lim would like to express his sincere appreciation to Professor E. Frömter of the Max-Planck-Institut für Biophysik in Frankfurt, Federal Republic of Germany for the kind generosity shown him during his stay in Professor Frömter's laboratory. Some of the voltage divider ratios and the computer acquired data were obtained in that laboratory.

This work was supported by National Institutes of Health research grant EY 01080 and Research Career Development award EY 00006 to Dr. Fischbarg, and by National Institutes of Health grant EY 02104 and award EY 00105 to Dr. Lim.

Received for publication 2 January 1981 and in revised form 7 July 1981.

REFERENCES

Anderson, E., J. Fischbarg, and A. Spector. 1973. Fluid transport, ATP level, and ATPase activities in isolated rabbit corneal endothelium. *Biochim. Biophys. Acta.* 307:557–562.

Barfort, P., and D. Maurice. 1974. Electrical potential and fluid transport across the corneal endothelium. *Exp. Eye Res.* 19:11–19.

Brown, A. C., and K. G. Kastella. 1965. The AC impedance of frog skin and its relation to active transport. *Biophys. J.* 5:591–606.

Clausen, C., S. A. Lewis, and J. M. Diamond. 1979. Impedance analysis of a tight epithelium using a distributed resistance model. *Biophys. J.* 26:291–318.

Cole, K. S. 1928. Electric impedance of suspensions of Arbacia eggs. *J. Gen. Physiol.* 12:37–54.

Cole, K. S., and R. F. Baker. 1941. Transverse impedance of the squid giant axon during current flow. *J. Gen. Physiol.* 24:535–549.

Cole, K. S. 1949. Some physical aspects of bioelectric phenomena. *Proc. Natl. Acad. Sci. U. S. A.* 35:558–566.

Cole, K. S. 1965. Electrodiffusion models for the membrane of squid giant axon. *Physiol. Rev.* 45:340–379.

Cole, K. S. 1968. Membranes, Ions, and Impulses. University of California Press, Berkeley and Los Angeles.

Dennis, W. H. 1959. Impedance of the gastric mucosa determined with a four electrode system. Dissertation, University of Louisville, Louisville, Ky.

Diamond, J. M., and W. H. Bossert. 1968. Functional consequences of ultrastructural geometry in "backwards" fluid-transporting epithelia. *J. Cell Biol.* 37:694–702.

Dikstein, S., and D. M. Maurice. 1972. The metabolic basis to the fluid pump in the cornea. *J. Physiol.* 221:29–41.

Fischbarg, J. 1972. Potential difference and fluid transport across rabbit corneal endothelium. *Biochim. Biophys. Acta.* 288:362–366.

Fischbarg, J. 1973. Active and passive properties of the rabbit corneal endothelium. *Exp. Eye Res.* 15:615–638.

Fischbarg, J., and J. J. Lim. 1973. Determination of the impedance locus of rabbit corneal endothelium. *Biophys. J.* 13:595–599.

Fischbarg, J., and J. J. Lim. 1974. Role of cations, anions, and carbonic anhydrase in fluid transport across rabbit corneal endothelium. *J. Physiol. (Lond.).* 241:647–675.

Fischbarg, J., C. R. Warshavsky, and J. J. Lim. 1977. Pathways for hydraulically and osmotically induced water flows across epithelia. *Nature (Lond.)*. 266:71–74.

Fischbarg, J., J. J. Lim, and J. Bourguet. 1977. Adenosine stimulation of fluid transport across rabbit corneal endothelium. *J. Membr. Biol.* 35:95–112.

Fischbarg, J. 1979. Pathways for water permeation across epithelia. *INSERM (Inst. Nat. Sante Rech. Med.) Symp.* 85:323–334.

Fricke, H. 1925. The electric capacity of suspensions with special reference to blood. *J. Gen. Physiol.* 9:137–152.

Frömter, E. 1972. The route of passive ion movement through the epithelium of Necturus gallbladder. *J. Membr. Biol.* 8:259–301.

Gögelein, H. 1980. Function analysis and impedance measurements in the gallbladder epithelium. Dissertation, Catholic University of Leuven, Leuven, Belgium.

Gögelein, H., and W. van Driessche. 1981. Capacitive and inductive low frequency impedances of Necturus gallbladder epithelium. *Pflügers Arch. Eur. J. Physiol.* 389:105–113.

Helman, S. I., and D. A. Miller. 1971. In vitro techniques for avoiding edge damage in studies of frog skin. *Science (Wash. D.C.)*. 173:146–148.

Hirsch, G., G. Renard, J.-P. Faure, and Y. Pouliquen. 1976. Formation of intercellular spaces and junctions in regenerating rabbit corneal endothelium. *Exp. Eye Res.* 23:385–397.

Hodson, S. 1974. The regulation of corneal hydration by a salt pump requiring the presence of sodium and bicarbonate ions. *J. Physiol. (Lond.)*. 236:271–302.

Hodson, S., and F. Miller. 1976. The bicarbonate ion pump in the endothelium which regulates the hydration of rabbit cornea. *J. Physiol. (Lond.)*. 263:563–577.

Hull, D. S., K. Green, M. Boyd, and G. R. Wynn. 1977. Corneal endothelium bicarbonate transport and effect of carbonic anhydrase inhibitors on endothelial permeability and fluxes and corneal thickness. *Invest. Ophthalmol.* 16:883–892.

Kay, G. I., and G. D. Pappas. 1962. Studies on the cornea. I. The fine structure of the rabbit cornea and the uptake and transport of colloidal particles by the cornea in vivo. *J. Cell Biol.* 12:457–479.

Klyce, S. D. 1972. Electrical profiles in the corneal epithelium. *J. Physiol. (Lond.)*. 226:407–429.

Klyce, S. D., and R. K. S. Wong. 1977. Site and mode of adrenaline action on chloride transport across the rabbit corneal epithelium. *J. Physiol. (Lond.)*. 266:777–799.

Lim, J. J., and J. Fischbarg. 1979. Intracellular potential of rabbit corneal endothelial cells. *Exp. Eye Res.* 28:619–626.

Lim, J. J., L. Kampmann, and E. Frömter. 1980. Fast intra- and transepithelial impedance measurements across a leaky epithelium. *Fed. Proc.* 39:1709. (Abstr.)

Lim, J. J., and H. H. Ussing. 1981. Analysis of presteady-state Na^+ fluxes across the rabbit corneal endothelium. *J. Membr. Biol.* In press.

Lim, J. J. 1981. Na^+ transport across the rabbit corneal endothelium. *Curr. Eye Res.* 1:255–258.

Maurice, D. M. 1951. The permeability to sodium ions of the living rabbit's cornea. *J. Physiol. (Lond.)*. 112:367–391.

Maurice, D. M. 1969. The cornea and sclera. *In* The Eye. H. Davson, editor. Academic Press, Inc., New York. 489–600.

Maurice, D. M. 1972. The location of the fluid pump in the cornea. *J. Physiol. (Lond.)*. 221:43–54.

Sandblom, J. 1972. Anomalous reactances in electrodiffusion systems. *Biophys. J.* 12:1118–1131.

Schifferdecker, H. and E. Frömter. 1978. The AC impedance of Necturus gallbladder epithelium. *Pflügers Archiv. Eur. J. Physiol.* 377:125–133.

Schwan, H. F. 1957. Electrical properties of tissue and cell suspensions. *Adv. Biol. Med. Phys.* 5:147–209.

Silver, G. A., J. Strauss, and G. A. Misrahy. 1965. Electrical impedance of isolated amnion. *Biophys. J.* 5:855–865.

Smith, P. G. 1971. The low-frequency electrical impedance of the isolated frog skin. *Acta Physiol. Scand.* 81:355–366.

Suzuki, K., V. Rohlicek, and E. Frömter. 1978. A quasi-totally shielded, low-capacitance glass-microelectrode with suitable amplifier for high-frequency intracellular potential and impedance measurements. *Pflügers Archiv. Eur. J. Physiol.* 378:141–148.

Teorell, T. 1949. Membrane electrophoresis in relation to bioelectrical polarization effects. *Arch. Sci. Physiol.* 3:205–219.

Wiederholt, M., and M. Koch. 1978. Intracellular potentials of isolated rabbit and human corneal endothelium. *Exp. Eye Res.* 21:511–518.